

Spin Distribution in Electron-Rich Piano-Stool Iron(III) Pyridylalkynyl Radical Cations Containing  $[(\eta^2\text{-dppe})(\eta^5\text{-C}_5\text{Me}_5)\text{FeC}\equiv\text{C}]^+$  End GroupsFrédéric Paul,<sup>\*,†</sup> Floriane Malvolti,<sup>†</sup> Grégory da Costa,<sup>‡</sup> Sylvie Le Stang,<sup>†</sup>  
Frédéric Justaud,<sup>†</sup> Gilles Argouarch,<sup>†</sup> Arnaud Bondon,<sup>\*,‡</sup> Sourisak Sinbandhit,<sup>§</sup>  
Karine Costuas,<sup>†</sup> Loïc Toupet,<sup>||</sup> and Claude Lapinte<sup>\*,†</sup><sup>†</sup>Sciences Chimiques de Rennes, UMR CNRS 6226, Université de Rennes 1, Campus de Beaulieu, Bât. 10C, F-35042 Rennes Cedex, France, <sup>‡</sup>PRISM, UMR CNRS 6026, Université de Rennes 1, CS 34317, Campus de Villejean, 35043 Rennes Cedex, France, <sup>§</sup>CRMPO, Université de Rennes 1, Campus de Beaulieu, 35042 Rennes Cedex, France, and <sup>||</sup>Institut de Physique de Rennes (IPR), UMR CNRS 6251, Université de Rennes 1, Campus de Beaulieu, F-35042 Rennes Cedex, France

Received March 3, 2010

This experimental and theoretical contribution is aimed at investigating the electronic structure of cationic electron-rich ethynylpyridyl Fe(III) derivatives of the formula  $[(\eta^2\text{-dppe})(\eta^5\text{-C}_5\text{Me}_5)\text{FeC}\equiv\text{C}(x\text{-C}_5\text{H}_4\text{N})][\text{PF}_6]$  ( $x = 4, 3, 2$ ; **1a–c** $[\text{PF}_6]$ ) and  $[(\eta^2\text{-dppe})(\eta^5\text{-C}_5\text{Me}_5)\text{FeC}\equiv\text{C}(2,5\text{-C}_5\text{H}_3\text{NX})][\text{PF}_6]$  ( $X = \text{Cl, Br}$ ; **2a,b** $[\text{PF}_6]$ ). The Mössbauer, NMR, and ESR characterization of these paramagnetic species are reported and discussed in connection with DFT results. Special emphasis is put on the electronic effect of the nitrogen atom and of the halogen substituent on the spin distribution within the pyridyl unit. It is shown that <sup>1</sup>H NMR constitutes a straightforward empirical way to investigate the slight changes in spin distribution taking place on the heteroaryl ring.

## Introduction

Pyridyl-based mono- or polydentate ligands incorporating electron-rich organometallic acetylide fragments have attracted considerable attention recently.<sup>1</sup> Upon complexation, such “metallo-ligands” possessing redox-active substituents should provide an easy access to various kinds of molecular architectures presenting unique properties for information storage or information processing at the molecular level.<sup>2</sup> We have previously

reported on compounds incorporating “ $(\eta^2\text{-dppe})(\eta^5\text{-C}_5\text{Me}_5)\text{FeC}\equiv\text{C}$ –” groups.<sup>3–5</sup> The simplest structurally among these organoiron metallo-ligands are the monodentate pyridylalkynyl complexes **1a–c**.<sup>6</sup> These Fe(II) compounds were fully characterized and shown to behave as functional pyridines toward various metal centers.<sup>5</sup> The corresponding Fe(III) complexes **1a–c** $[\text{PF}_6]$  were also previously isolated and briefly characterized. These species were shown to be weaker ligands than the equivalent Fe(II) complexes.<sup>5</sup> More recently, the related Fe(II) compounds **2a,b**, featuring a halogen in a position ortho to the nitrogen, were synthesized (Chart 1) and used as precursors to access new bipyridine ligands functionalized with two Fe(II) redox-active groups.<sup>3</sup> However, the corresponding Fe(III) complexes **2a,b** $[\text{PF}_6]$  have not been characterized so far. Thus, in comparison to functional phenylacetylide Fe(III) complexes such as **3-X** $[\text{PF}_6]$  (Chart 1), relatively few data are available regarding the pyridyl-based Fe(III) analogues.<sup>7–10</sup> Such a knowledge is, however, crucial when optimal tuning of a given electronic property of functional assemblies made from these compounds is sought.

\*To whom correspondence should be addressed. F.P. and C.L.: tel, (+33) 02 23 23 59 62; fax, (+33) 02 23 23 56 37. A.B.: tel, (+33) 2 23 23 65 61; fax, (+33) 2 23 23 46 06.

(1) (a) Koutsantonis, G. A.; Jenkins, G. I.; Schauer, P. A.; Szczepaniak, B.; Skelton, B. W.; Tan, C.; White, A. H. *Organometallics* **2009**, *28*, 2195–2205. (b) Ge, Q.; Corkery, T. C.; Humphrey, M. G.; Samoc, M.; Hor, T. S. A. *Dalton Trans.* **2009**, 6192–6200. (c) Muro, M. L.; Diring, S.; Wang, X.; Ziesel, R.; Castellano, F. N. *Inorg. Chem.* **2008**, *47*, 6796–6803. (d) Muro, M. L.; Diring, S.; Wang, X.; Ziesel, R.; Castellano, F. N. *Inorg. Chem.* **2009**, *48*, 11533–11542. (e) Cifuentes, M. P.; Humphrey, M. G.; Koutsantonis, G. A.; Lengkeek, N. A.; Petrie, S.; Sanford, V.; Schauer, P. A.; Skelton, B. W.; Stranger, R.; White, A. H. *Organometallics* **2008**, *27*, 1716–1726. (f) Pélerin, O.; Olivier, C.; Roisnel, T.; Touchard, D.; Rigaut, S. *J. Organomet. Chem.* **2008**, *693*, 2153–2158. (g) Xu, H.-B.; Zhang, L.-Y.; Xie, Z.-L.; Ma, E.; Chen, Z.-N. *Chem. Commun.* **2007**, 2744–2746. (h) Wong, C.-Y.; Tong, G. S. M.; Che, C.-M.; Zhu, N. *Angew. Chem., Int. Ed.* **2006**, *45*, 2694–2698. (i) Méry, D.; Omelas, C.; Daniel, M.-C.; Ruiz, J.; Rodrigues, J.; Astruc, D.; Cordier, S.; Kirakci, K.; Perrin, C. *R. Chim.* **2005**, *8*, 1789–1797. (j) Kühn, F. E.; Zuo, J.-L.; de Biani, F. F.; Santos, A. M.; Zhang, Y.; Zhao, J.; Sandulache, A.; Herdtweck, E. *New J. Chem.* **2004**, *28*, 43–51. (k) Engratkul, C.; Schoemaker, W. J.; Grzybowski, J. J.; Guzei, I.; Rheingold, A. *Inorg. Chem.* **2000**, *39*, 5161–5163.

(2) (a) Balzani, V.; de Silva, A. P. *Electron Transfer in Chemistry*; Wiley-VCH: Weinheim, Germany, 2000; Vol. 5. (b) Norgaard, K.; Bjornholm, T. *Chem. Commun.* **2005**, 1812–1823. (c) Gianneschi, N. C.; Masar, M. S., III; Mirkin, C. A. *Acc. Chem. Res.* **2005**, *38*, 825–837. (d) Lehn, J.-M. *Angew. Chem., Int. Ed. Engl.* **1990**, *29*, 1304–1319. (e) Lehn, J. M. *Supramolecular Chemistry-Concepts and Perspectives*; VCH: Weinheim, Germany, 1995.

(3) Justaud, F.; Argouarch, G.; Gazalah, S. I.; Toupet, L.; Paul, F.; Lapinte, C. *Organometallics* **2008**, *27*, 4260–4264.

(4) (a) Ibn Ghazala, S.; Gauthier, N.; Paul, F.; Toupet, L.; Lapinte, C. *Organometallics* **2007**, *26*, 2308–2317. (b) Paul, F.; Goeb, S.; Justaud, F.; Argouarch, G.; Toupet, L.; Ziesel, R. F.; Lapinte, C. *Inorg. Chem.* **2007**, *46*, 9036–9038.

(5) Le Stang, S.; Paul, F.; Lapinte, C. *Inorg. Chim. Acta* **1999**, *291*, 403–425.

(6) Le Stang, S.; Lenz, D.; Paul, F.; Lapinte, C. *J. Organomet. Chem.* **1998**, *572*, 189–192.

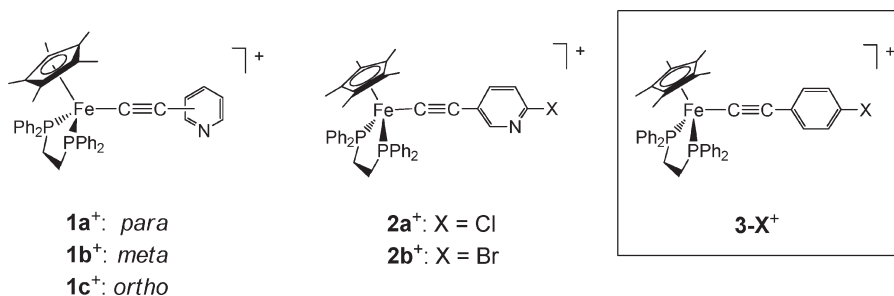
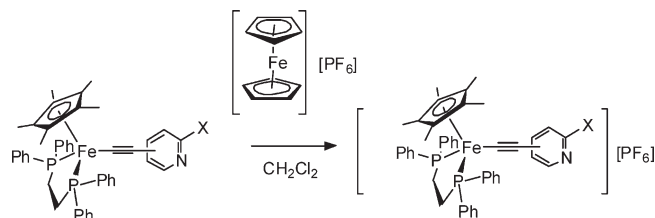
(7) Paul, F.; da Costa, G.; Bondon, A.; Gauthier, N.; Sinbandhit, S.; Toupet, L.; Costuas, K.; Halet, J.-F.; Lapinte, C. *Organometallics* **2007**, *26*, 874–896.

(8) Paul, F.; Toupet, L.; Thépot, J.-Y.; Costuas, K.; Halet, J.-F.; Lapinte, C. *Organometallics* **2005**, *24*, 5464–5478.

(9) Costuas, K.; Paul, F.; Toupet, L.; Halet, J.-F.; Lapinte, C. *Organometallics* **2004**, *23*, 2053–2068.

(10) Denis, R.; Toupet, L.; Paul, F.; Lapinte, C. *Organometallics* **2000**, *19*, 4240–4251.

Chart 1. Selected Pyridyl- and Aryl-Based Fe(III) Complexes

Scheme 1. Oxidation of the Fe(II) Complexes **1a–c** and **2a,b**

In the present contribution, we have therefore performed the extensive spectroscopic characterization of **1a–c**[PF<sub>6</sub>] and **2a,b**[PF<sub>6</sub>]. A density functional theory (DFT) study was also undertaken in order to complete our understanding of the electronic structures of these open-shell derivatives, particular attention being paid to the influence of the nitrogen atom and/or of the halogen substituent on the spin distribution.

## Results

**Synthesis of the Fe(III) Complexes.** The precursor Fe(II) compounds **1a–c** and **2a,b** were synthesized according to previously published procedures and subsequently oxidized following the “classic” workup (Scheme 1) to give the desired corresponding Fe(III) complexes.<sup>3,5,6</sup> The purity of the known Fe(III) samples **1a–c**[PF<sub>6</sub>] was checked by electrochemistry and IR spectroscopy, while the new compounds **2a,b**[PF<sub>6</sub>] were fully characterized by the usual means (Experimental Section). The latter exhibit characteristic spectroscopic signatures very similar to these previously observed for **1b**[PF<sub>6</sub>].<sup>5</sup> Thus, they possess low-intensity charge transfer bands in the visible range presumed to be LMCT bands, an absorption of weak intensity in the near-IR range, presumably corresponding to a symmetry-forbidden LF transition with a strong d–d character,<sup>8</sup> and also two IR vibrational modes of very low intensity in the 1940–2010 cm<sup>-1</sup> spectral region, one of which (or both in case of Fermi coupling)<sup>11</sup> corresponds to  $\nu_{C\equiv C}$ .<sup>5</sup>

**Solid-State Structures of **2a,b**[PF<sub>6</sub>].** In the course of these syntheses, the new Fe(III) compounds **2a,b**[PF<sub>6</sub>] could be crystallized, and their solid-state structures were solved by X-ray diffraction (Figure 1; see also Table 6 in the Experimental Section). To our knowledge, these structural data are the first for piano-stool Fe(III) pyridylalkynyl complexes. Crystal data and space groups are similar for both compounds (Table 6), as is the conformation adopted by the single molecule in the asymmetric unit. In line with published data,<sup>12</sup> the carbon–

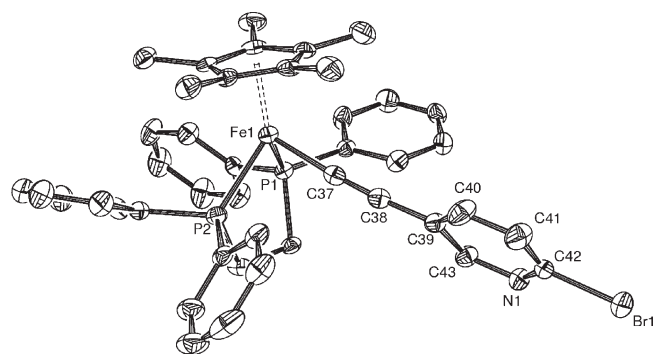


**Figure 1.** ORTEP representations of the cation **2b<sup>+</sup>** at the 50% probability level. Selected distances (Å) and angles (deg) for **2b**[PF<sub>6</sub>]: Fe1–(Cp\*)<sub>centroid</sub> = 1.779, Fe1–P1 = 2.2515(10), Fe1–P2 = 2.2508(9), Fe1–C37 = 1.889(3), C37–C38 = 1.207(4), C38–C39 = 1.440(3), C39–C40 = 1.389(5), C40–C41 = 1.378(4), C41–C42 = 1.369(5), C39–C43 = 1.395(4), N1–C42 = 1.321(4), N1–C43 = 1.330(4), Br1–C42 = 1.903(3); P1–Fe1–P2 = 83.51(4), Fe1–C37–C38 = 175.5(3), C37–C38–C39 = 176.2(3), C43–C39–Fe1–(Cp\*)<sub>centroid</sub> = –136.7.<sup>13</sup>

**Table 1.** <sup>57</sup>Fe Mössbauer Fitting Parameters at 80 K for Selected Complexes

compd	IS (±0.01 mm s <sup>-1</sup> )	QS (±0.01 mm s <sup>-1</sup> )	Γ (mm s <sup>-1</sup> ) <sup>a</sup>	area (%)
<b>1a</b>	0.24	1.95	0.11	100
<b>1a</b> [PF <sub>6</sub> ]	0.25	0.91	0.15	100
<b>1b</b>	0.25	1.90	0.12	100
<b>1b</b> [PF <sub>6</sub> ] <sup>b</sup>	0.25	0.87	0.16	57
<b>1c</b>	0.24	1.87	0.12	100
<b>1c</b> [PF <sub>6</sub> ]	0.23	0.92	0.15	100

<sup>a</sup> Half-width of the peaks of the signal. <sup>b</sup> Two other doublets present at isomeric shifts of 0.13 mm s<sup>-1</sup> (29%; QS = 1.22 ± 0.03 mm s<sup>-1</sup>) and of 0.21 mm s<sup>-1</sup> (14%; QS = 1.92 ± 0.02 mm s<sup>-1</sup>).

bromine bond C42–Br1 of **2b**[PF<sub>6</sub>] is ca. 0.15 Å longer than the carbon–chlorine bond C42–Cl1 of **2a**[PF<sub>6</sub>] (1.903(3) vs 1.741(2) Å). Relative to their respective Fe(II) parents **2a,b**,<sup>3</sup> the changes in bond lengths upon oxidation are very similar to these previously observed for related **3-X/3-X**[PF<sub>6</sub>] systems.<sup>8,10</sup> Thus, a slight shortening of the Fe–C37 bond and of the C42–X1 (X = Cl, Br) bonds, along with a slight elongation of the Fe1–P1, Fe1–P2, and Fe1–(C<sub>5</sub>Me<sub>5</sub>) bonds are

(13) Selected distances (Å) and angles (deg) for **2a**[PF<sub>6</sub>]: Fe1–(Cp\*)<sub>centroid</sub> = 1.774, Fe1–P1 = 2.2460(6), Fe1–P2 = 2.2446(5), Fe1–C37 = 1.8800(19), C37–C38 = 1.216(3), C38–C39 = 1.435(3), C39–C40 = 1.396(3), C40–C41 = 1.378(3), C41–C42 = 1.374(3), C39–C43 = 1.374(3), N1–C42 = 1.328(2), N1–C43 = 1.328(2), Cl1–C42 = 1.741(2); P1–Fe1–P2 = 83.40(2), Fe1–C37–C38 = 173.9(2), C37–C38–C39 = 176.7(2), C43–C39–Fe1–(Cp\*)<sub>centroid</sub> = –139.8.

(11) Paul, F.; Mevellec, J.-Y.; Lapinte, C. *Dalton Trans.* **2002**, 1783–1790.  
 (12) Allen, F. H.; Kennard, O.; Watson, D. G.; Brammer, L.; Orpen, A. G.; Taylor, R. *J. Chem. Soc., Perkin Trans. 2* **1987**, S1–S19.

observed, the rest of the bond lengths remaining fairly constant within experimental uncertainties (Supporting Information).

**Mössbauer Characterization of 1a–c and 1a–c[PF<sub>6</sub>].** The pyridyl complexes were then characterized by <sup>57</sup>Fe Mössbauer spectrometry at 80 K in their neutral Fe(II) (1a–c) and radical cation Fe(III) (1a–c[PF<sub>6</sub>]) states. The characteristic doublets expected for these compounds were always detected as the sole signal, except for 1b[PF<sub>6</sub>] (Table 1).<sup>14</sup> In this case, two additional doublets of lower intensities were also detected. These presumably originate from iron-containing species which result from partial decomposition of this reactive Fe(III) sample. The isomeric shifts (IS) of the Fe(II) (1a–c) and Fe(III) samples (1a–c[PF<sub>6</sub>]) remain quite close and are not very sensitive to the nature of the pyridyl ring or to the redox state of the iron center for a given isomer. In contrast, the quadrupolar splitting (QS) is clearly diagnostic of the redox state of the metal center, QS values of around 0.9 mm s<sup>-1</sup> being observed for Fe(III) complexes, while QS values closer to 1.9 mm s<sup>-1</sup> are observed for Fe(II) complexes.<sup>15,16</sup> Overall, these results are reminiscent of those previously reported for the 3-X<sup>+</sup> alkyne complexes (Chart 1).<sup>10</sup> The similarities of the IS and QS parameters obtained for both Fe(II) and Fe(III), whatever the position of the nitrogen on the aromatic ring, clearly indicate that the electronic environment of the iron nucleus is not sensitive to the structure of the pyridylalkynyl ligand.

**Table 2. Experimental ESR *g* Values<sup>a</sup> and Redox Potentials<sup>b,c</sup> for 1a–c[PF<sub>6</sub>] and 2a,b[PF<sub>6</sub>] and computed *g* Values and Ionization Potentials for 1a–c-H<sup>+</sup><sup>d</sup>**

compd	<i>g</i> <sub>1</sub>	<i>g</i> <sub>2</sub>	<i>g</i> <sub>3</sub>	< <i>g</i> >	Δ <i>g</i>	<i>E</i> <sup>o</sup> (V)	IP <sup>o</sup> (eV) <sup>c</sup>
1a <sup>+</sup>	1.969	2.028	2.494	2.163	0.525	-0.03 <sup>b</sup>	
1b <sup>+</sup>	1.967	2.028	2.490	2.162	0.521	-0.11 <sup>b</sup>	
1c <sup>+</sup>	1.966	2.024	2.500	2.163	0.534	-0.08 <sup>b</sup>	
2a <sup>+</sup>	1.967	2.027	2.503	2.165	0.536	-0.07 <sup>c</sup>	
2b <sup>+</sup>	1.972	2.028	2.509	2.169	0.537	-0.06 <sup>c</sup>	
1a-H <sup>+</sup> <sup>d</sup>	1.990	2.040	2.162	2.064	0.172		6.190
1b-H <sup>+</sup> <sup>d</sup>	1.992	2.036	2.137	2.055	0.145		6.008
1c-H <sup>+</sup> <sup>d</sup>	1.990	2.038	2.173	2.067	0.183		5.915

<sup>a</sup> Experimental ESR *g* values (±0.005) determined at 77 K in CH<sub>2</sub>Cl<sub>2</sub>/C<sub>2</sub>H<sub>4</sub>Cl<sub>2</sub> (1/1) glass. <sup>b</sup> Values from ref 5. <sup>c</sup> Values from ref 3. <sup>d</sup> Computed *g*-tensor values and ionization potentials (IP) for the model compounds 1a–c-H<sup>+</sup> are reported for the sake of comparison.

**ESR of the Fe(III) Complexes 1a–c[PF<sub>6</sub>] and 2a,b[PF<sub>6</sub>].** The five Fe(III) complexes were characterized by ESR. A rhombic signal was detected for each of them in solvent glasses at 80 K (Figure 2 and Table 2).<sup>8,15</sup> In accordance with the conclusion drawn from the Mössbauer data, the ESR data suggest that the main features of the HOMO are not very sensitive to the structure of the pyridylalkynyl ligand (see Figure 6). Indeed, the mean *g* values and the anisotropy (Δ*g*) of the detected signals remain sensibly similar for 1a[PF<sub>6</sub>] and 1b[PF<sub>6</sub>], a slight increase in Δ*g* taking place for 1c[PF<sub>6</sub>]. However, the data for 2a,b[PF<sub>6</sub>] reveal that an increase of the anisotropy takes place relative to 1b[PF<sub>6</sub>] when a halogen substituent is appended in a position para to the acetylide linker.

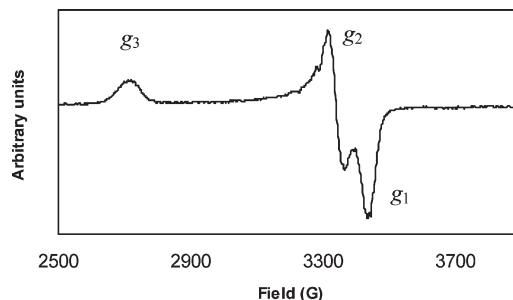


**Figure 2.** ESR spectrum of 1a<sup>+</sup> in a CH<sub>2</sub>Cl<sub>2</sub>/1,2-C<sub>2</sub>H<sub>4</sub>Cl<sub>2</sub> (1/1) glass at 80 K.

**NMR of the Fe(III) Complexes 1a–c[PF<sub>6</sub>] and 2a,b[PF<sub>6</sub>].** The <sup>1</sup>H NMR spectra of 1a–c[PF<sub>6</sub>] and 2a,b[PF<sub>6</sub>] have subsequently been recorded in dichloromethane-*d*<sub>2</sub> (Figure 3). The <sup>1</sup>H NMR signals were detected in ranges similar to those of the known Fe(III) radicals 3-X[PF<sub>6</sub>] (Table 3).<sup>7</sup>

Our first trial was to assign the various <sup>1</sup>H signals detected. For 1a[PF<sub>6</sub>], this proved possible by monitoring the <sup>1</sup>H NMR shifts of various mixtures of 1a/1a[PF<sub>6</sub>] as a function of the Fe(II) composition of the sample (Figure 4). In line with previous studies on such Fe(III) radical cations,<sup>7,17</sup> the electron self-exchange reaction is much faster than the <sup>1</sup>H NMR chemical shift time scale and an averaged set of signals is always observed. A progressive increase in the concentration of the paramagnetic complex 1a[PF<sub>6</sub>] thereby allows firm identification of most of the signals detected for the Fe(III) samples, on the basis of their assignment in the spectra of the diamagnetic Fe(II) samples.

As for 3-X[PF<sub>6</sub>] compounds, rather specific <sup>1</sup>H NMR shifts are observed for the “(η<sup>2</sup>-dppe)(η<sup>5</sup>-C<sub>5</sub>Me<sub>5</sub>)Fe” fragment (Figure 3). Thus, the C<sub>5</sub>Me<sub>5</sub> protons (H<sub>9</sub>) give rise to the most intense peak of the spectrum near -10 ppm, while the endo and exo phenyl protons (H<sub>1</sub>/H<sub>2</sub>/H<sub>3</sub> and H<sub>4</sub>/H<sub>5</sub>/H<sub>6</sub>) of the dppe ligand appear in the diamagnetic range as two characteristic sets of signals in a roughly 2/2/1 ratio. The assignment of these sets of signals was also confirmed by COSY experiments. Assignment of the endo and exo sets was made by analogy with 3-X[PF<sub>6</sub>] compounds.<sup>7</sup> Among the methylene protons H<sub>7</sub> and H<sub>8</sub>, the latter come out slightly below -3 ppm, while the former is often not detected but is believed to be in the 5–9 ppm range, presumably hidden below the aromatic dppe protons. Finally, the pyridyl protons of 1a[PF<sub>6</sub>] correspond to the most shifted signals and were detected around the -23 ppm range (H<sub>a</sub>) and around 25 ppm (H<sub>b</sub>). Protons ortho and para to the acetylide bridge are shifted to high field, while meta protons are shifted to low field, in line with the observations previously made for 3-X[PF<sub>6</sub>] species.<sup>7</sup> The assignment of the various pyridyl protons of 1a[PF<sub>6</sub>] was further confirmed by polarization transfer studies.

For the other isomers of 1a[PF<sub>6</sub>], the signals of the protons belonging to the “(η<sup>2</sup>-dppe)(η<sup>5</sup>-C<sub>5</sub>Me<sub>5</sub>)Fe” fragment were also readily identified on the basis of their characteristic shifts and intensities. The remaining signals, which are again the most shifted ones, correspond to the pyridyl protons. On the basis of the study of 3-X[PF<sub>6</sub>] complexes,<sup>7</sup> the most shifted signals at low field should correspond to hydrogen atoms in meta positions relative to the alkyne bridge, whereas those at high field correspond to hydrogen atoms

(14) (a) Greenwood, N. N. *Mössbauer Spectroscopy*; Chapman and Hall: London, 1971; (b) Güttlich, P.; Link, R.; Trautwein, A. In *Inorganic Chemistry Concepts. Mössbauer Spectroscopy and Transition Metal Chemistry*; Güttlich, P., Link, R., Trautwein, A., Eds.; Springer-Verlag: Berlin, 1978; Vol. 3, pp 191–201.

(15) Paul, F.; Lapinte, C. *Coord. Chem. Rev.* **1998**, 178/180, 431–509.

(16) Guillaume, V.; Thomiot, P.; Coat, F.; Mari, A.; Lapinte, C. *J. Organomet. Chem.* **1998**, 565, 75–80.

(17) Roger, C.; Hamon, P.; Toupet, L.; Rabaâ, H.; Saillard, J.-Y.; Hamon, J.-R.; Lapinte, C. *Organometallics* **1991**, 10, 1045–1054.

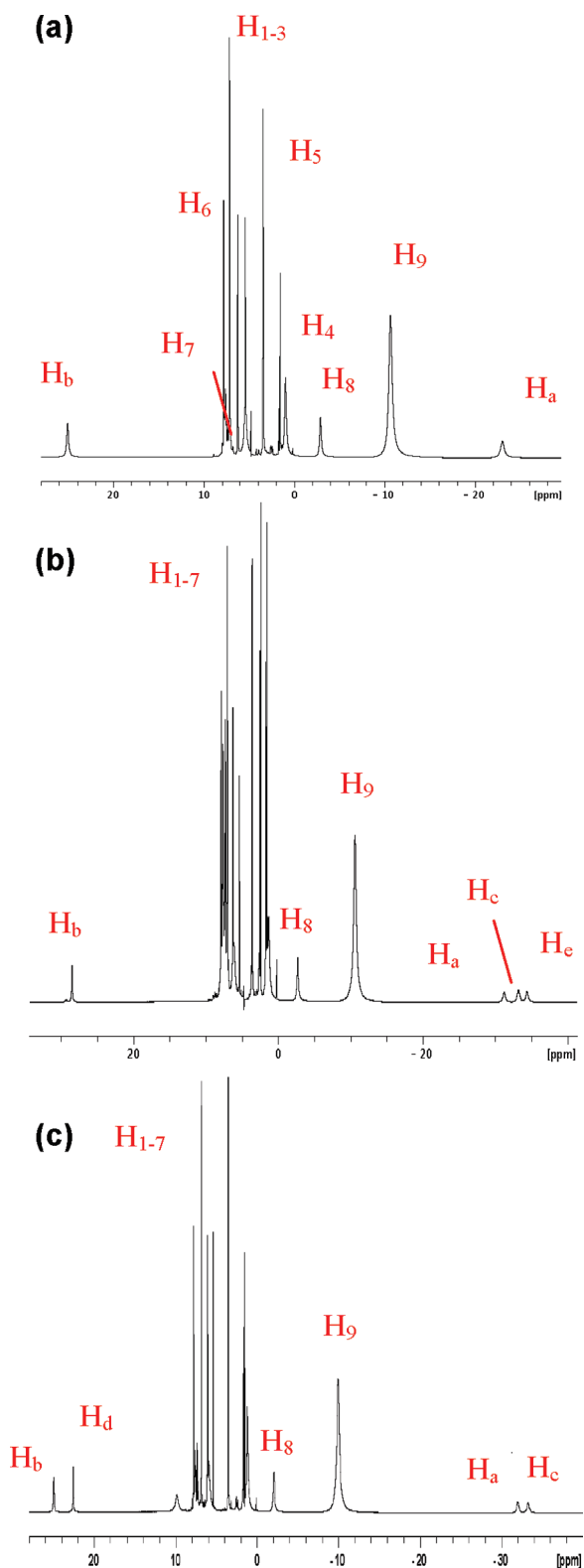


**Figure 3.**  $^1\text{H}$  NMR spectra of (a)  $1\text{a}[\text{PF}_6]$ , (b)  $1\text{b}[\text{PF}_6]$ , and (c)  $1\text{c}[\text{PF}_6]$  in  $\text{CD}_2\text{Cl}_2$  at  $25^\circ\text{C}$  with proposed assignments for selected protons according to Chart 2.

in para and ortho positions. This was what we observed for  $1\text{b},\text{c}[\text{PF}_6]$  and  $2\text{a},\text{b}[\text{PF}_6]$ , but no more precise assignment could be gained from the study of Fe(II)/Fe(III) mixtures. We had therefore to resort to polarization transfer studies to assign these signals. For  $1\text{c}[\text{PF}_6]$ , an unambiguous assignment proved possible from COSY correlations, since it

allowed us to differentiate the pyridyl protons  $\text{H}_b$  from  $\text{H}_d$  at low field and  $\text{H}_a$  from  $\text{H}_c$  at high field (Supporting Information). For  $1\text{b}[\text{PF}_6]$ , things were not so straightforward, because even if the COSY correlation allowed us to distinguish the signals corresponding to  $\text{H}_a$  and  $\text{H}_c$  from that of  $\text{H}_e$  in the set of signals at high field, it did not allow their particular assignment. The definitive assignment of  $\text{H}_a$  and  $\text{H}_c$  was eventually made by comparing the  $^1\text{H}$  NMR spectrum of  $1\text{b}[\text{PF}_6]$  with those of  $2\text{a},\text{b}[\text{PF}_6]$ , in which  $\text{H}_c$  has been replaced by X ( $\text{X} = \text{Cl}, \text{Br}$ ). Indeed, the spectra of the last two complexes closely resemble that of  $1\text{b}[\text{PF}_6]$  but lack a signal at high field. The latter was therefore assigned to  $\text{H}_c$  in  $1\text{b}[\text{PF}_6]$ .

The  $^{13}\text{C}$  NMR spectra of  $1\text{a}-\text{c}[\text{PF}_6]$  and  $2\text{a},\text{b}[\text{PF}_6]$  have also been recorded, and a tentative assignment of the detected signals is proposed on the basis of the previous investigation on  $3-\text{X}[\text{PF}_6]$  analogues (Supporting Information).<sup>7</sup> Likewise, we have assumed that none of the  $\alpha$ -acetylide carbon atoms ( $\text{C}_a$  in Chart 2) have presently been detected, and in some cases also not the  $\beta$  atoms ( $\text{C}_b$ ), which are expected to appear at very low fields. With the exception of the ipso aryl carbon atoms of the dppe ligand, which were previously also suspected to escape detection,<sup>7</sup> all carbon atoms belonging to the “ $(\eta^2\text{-dppe})(\eta^5\text{-C}_5\text{Me}_5)\text{-Fe}$ ” fragment were always identified from their characteristic shifts, many of these assignments being confirmed by HMQC correlations. The remaining signals were thus considered to belong to the pyridyl carbon atoms.<sup>18</sup>

**Temperature Dependence of the  $^1\text{H}$  NMR Signals.** We have then examined the temperature dependence of the  $^1\text{H}$  NMR shifts of  $1\text{a}-\text{c}[\text{PF}_6]$  between 300 and 180 K (Figure 5 and the Supporting Information). Similarly to  $3-\text{X}[\text{PF}_6]$  monoradicals,<sup>7</sup> a linear  $1/T$  dependence can be evidenced for the paramagnetic shifts ( $\delta_{\text{iso}}$ ) with very good fits for all nuclei, as apparent in Figure 5 (Curie behavior).<sup>19</sup> This behavior suggests that the ground state (GS) of these organometallic radicals has no closely lying excited states originating from spin-orbit coupling. As previously discussed,<sup>7</sup> the extrapolated values at infinite  $T$  for several of these shifts differ somewhat from the ideal “diamagnetic” values, which should be those of the corresponding Fe(II) parents ( $1\text{a}-\text{c}$ ). This possibly happens because the weak pseudocontact contribution to these particular isotropic shifts does not strictly follow a Curie law, in contrast to the assumption made in eq 2 (see hereafter), and consequently leads to the observed deviation upon extrapolation.

**Derivation of Hyperfine Coupling Constants and Spin Densities for the Primary Carbon Atoms of the Bridge of  $1\text{a}[\text{PF}_6]$ ,  $1\text{b}[\text{PF}_6]$ ,  $1\text{c}[\text{PF}_6]$  and  $2[\text{PF}_6]$ .** Likewise to what has been previously done for the  $3-\text{X}[\text{PF}_6]$  radical cations,<sup>7</sup> the contact hyperfine coupling constants and the spin densities were derived for selected protons of the pyridylalkynyl linker from the  $^1\text{H}$  NMR contact shifts (Supporting Information).

The NMR shift of a paramagnetic compound (eq 1a) is the sum of a diamagnetic contribution ( $\delta_{\text{dia}}$ ) and of an isotropic contribution ( $\delta_{\text{iso}}$ ), the latter actually originating from the

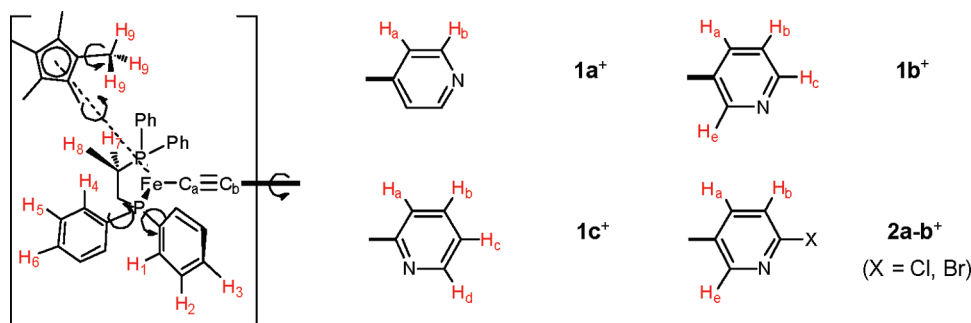
(18) However, the modest paramagnetic shifts of several among these signals call for caution until additional NMR data are available on this class of compounds. Indeed, some of these signals might equally correspond to diamagnetic impurities issued from a slow decomposition of the Fe(III) radicals in the  $\text{CD}_2\text{Cl}_2$ .

(19) (a) Bertini, I.; Galas, O.; Luchinat, C.; Parigi, G.; Spina, G. *J. Magn. Reson.* **1998**, *130*, 33–44. (b) Golding, R. M.; Pascual, R. O.; Vrbancich, J. *Mol. Phys.* **1976**, *31*, 731–744.

**Table 3.** Detected ( $\delta$ ) and Isotropic ( $\delta_{\text{iso}}$ )  $^1\text{H}$  NMR shifts ( $\delta \pm 0.1$  ppm) Recorded for  $1\text{a-c}[\text{PF}_6]$  and  $2\text{a,b}[\text{PF}_6]$  at 20 °C in  $\text{CD}_2\text{Cl}_2^a$ 

compd	$\delta$ (ppm)	-C≡C(C <sub>5</sub> H <sub>3</sub> NX)-				dppe								C <sub>5</sub> Me <sub>5</sub>	
		H <sub>a</sub>	H <sub>b</sub>	H <sub>c</sub>	H <sub>d</sub>	H <sub>e</sub>	H <sub>1</sub>	H <sub>2</sub>	H <sub>3</sub>	H <sub>4</sub>	H <sub>5</sub>	H <sub>6</sub>	H <sub>7</sub>	H <sub>8</sub>	H <sub>9</sub>
<b>1a</b> [PF <sub>6</sub> ] (X = H)	$\delta$	-23.1	25.1				5.3	7.1	6.2	0.9	3.4	7.9	n.o. <sup>b</sup>	-2.9	-10.7
	$\delta_{\text{iso}}$	-29.7	17.0				-2.3	-0.2	-1.1	-6.4	-3.9	0.6		-4.9	-12.1
<b>1b</b> [PF <sub>6</sub> ] (X = H)	$\delta$	-31.2	28.4	-33.2		-34.4	6.0	7.1	6.2	1.2	3.7	7.8	n.o. <sup>b</sup>	-2.8	-10.7
	$\delta_{\text{iso}}$	-38.2	21.4	-41.3		-42.5	-1.8	-0.2	-1.1	-6.1	-3.6	0.5		-4.8	-12.1
<b>1c</b> [PF <sub>6</sub> ] (X = H)	$\delta$	-32.0	25.0	-33.3	22.6		5.9	6.8	6.1	1.2	3.5	7.8	9.9 <sup>c</sup>	-2.1	-10.0
	$\delta_{\text{iso}}$	-39.3	17.7	-40.0	14.3		-0.5	-1.2	-6.1	-3.8	0.5	7.1	7.1	-4.1	-11.5
<b>2a</b> [PF <sub>6</sub> ] (X = Cl)	$\delta$	-29.7	28.6			-35.2	5.7	7.0	6.2	0.9	3.4	7.8	n.o. <sup>b</sup>	-3.0	-10.7
	$\delta_{\text{iso}}$	-37.0	21.3			-42.0	-2.1	-0.3	-1.1	-6.4	-3.9	0.5		-4.8	-12.2
<b>2b</b> [PF <sub>6</sub> ] (X = Br)	$\delta$	-29.4	28.7			-34.5	5.7	7.1	6.2	0.9	3.5	7.8	n.o. <sup>b</sup>	-3.0	-10.7
	$\delta_{\text{iso}}$	-36.7	21.4			-41.3	-2.1	-0.2	-1.1	-6.4	-3.8	0.5		-4.8	-12.2

<sup>a</sup> Proposed assignment according to Chart 2 (CHDCl<sub>2</sub> at 5.35 ppm). <sup>b</sup> Not observed. <sup>c</sup> Tentative assignment.

**Chart 2.**  $^1\text{H}$  Nuclei Numeration Corresponding to the Proposed Assignment for  $1\text{a-c}[\text{PF}_6]$  and  $2\text{a,b}[\text{PF}_6]$ 

presence of the electronic spin of the unpaired electron(s).<sup>20</sup> This contribution (eq 1b) is itself the sum of a contact ( $\delta_c$ ) and a pseudocontact term ( $\delta_{\text{pc}}$ ).

$$\delta_{\text{obs}} = \delta_{\text{dia}} + \delta_{\text{iso}} \quad (1a)$$

$$\delta_{\text{iso}} = \delta_c + \delta_{\text{pc}} \quad (1b)$$

$$\delta_{\text{pc}} = (\delta_{\text{pc}})^{\text{M}} + (\delta_{\text{pc}})^{\text{L}} \quad (1c)$$

As shown in eq 1c, the pseudocontact shift is also the sum of two contributions. The second one, called the ligand-centered term ( $\delta_{\text{pc}}^{\text{L}}$ ), can be neglected for hydrogen nuclei in complexes where the unpaired electron mostly resides on the metal center. The pseudocontact contribution to the isotropic shift therefore results essentially from the first term, which represents the metal-centered term ( $\delta_{\text{pc}}^{\text{M}}$ ). This contribution can be roughly evaluated (eq 2), provided the diagonal values of the  $\mathbf{g}$  tensor and some geometrical features of these Fe(III) radicals are known.<sup>7</sup> In this equation,  $\mu_0$  is the vacuum permittivity,  $\mu_{\text{B}}$  is the Bohr magneton,  $k$  is the Boltzmann constant,  $S$  is the spin of the radical ( $S = 1/2$ ),  $g_{\parallel}$  is  $g_3$ ,  $g_{\perp}$  is the average of  $g_1$  and  $g_2$  (Table 2),  $r_{\text{M}}$  is the distance between the metal center and the proton considered, while  $\theta$  is the angle between  $r_{\text{M}}$  and the acetylide axis.

$$(\delta_{\text{pc}})^{\text{M}} = (\mu_0/4\pi)(\mu_{\text{B}}^2/9kT)[S(S+1)](g_{\parallel}^2 - g_{\perp}^2)(3 \cos^2 \theta - 1)/r_{\text{M}}^3 \quad (2)$$

This contribution was computed for  $1\text{a-c}[\text{PF}_6]$  and  $2\text{a,b}[\text{PF}_6]$ , using the geometrical parameters of the corresponding Fe(II) complexes ( $1\text{a-c}$ ) for  $1\text{a-c}[\text{PF}_6]$  and those determined by

(20) Bertini, I.; Luchinat, C. *NMR of Paramagnetic Molecules in Biological Systems*; Benjamin/Cummings: Menlo Park, CA, 1986.

**Table 4.**  $\pi$ -Spin Densities on Primary Pyridyl Carbon Atoms Derived from the  $^1\text{H}$  NMR Contact Shifts of the Nearby Protons using the McConnell Relationship (eq 4) for  $1\text{a-c}[\text{PF}_6]$  and  $2\text{a,b}[\text{PF}_6]$  at 295 K

compd	$(\rho^{\pi})_{\text{C}}^a$ for pyridyl C(H) atoms				
	C <sub>d</sub>	C <sub>e</sub>	C <sub>f/N</sub>	C <sub>g/N</sub>	C <sub>h/N</sub>
<b>1a</b> [PF <sub>6</sub> ]	0.018	-0.008			
<b>1b</b> [PF <sub>6</sub> ]	0.022	-0.010	0.023		0.025
<b>1c</b> [PF <sub>6</sub> ]	0.024	-0.008	0.022	-0.007	
<b>2a</b> [PF <sub>6</sub> ]	0.022	-0.010			0.025
<b>2b</b> [PF <sub>6</sub> ]	0.022	-0.010			0.024

<sup>a</sup>  $\pi$ -spin densities expressed in electrons (e) for carbon atoms numbered according to Chart 3.

X-ray for  $2\text{a,b}[\text{PF}_6]$ ,<sup>21</sup> and subsequently deduced from the isotropic shift of each proton to give the corresponding contact shift ( $\delta_c$ ). From these contact shifts, the contact contribution to the isotropic hyperfine constants ( $A_{\text{H}}^{\text{con}}$ ) was in turn computed with eq 3. In this equation,  $\gamma_{\text{H}}$  is the proton magnetogyric ratio,  $\hbar$  is the reduced Planck constant, and  $g$  is the mean electron  $g$  value (Table 2), while other constants have been previously defined. Finally, the McConnell expression (eq 4) provides a straightforward access to the spin density on the nearby carbon atom from this contact hyperfine coupling for these  $S = 1/2$  radicals (Table 4).<sup>22</sup> Interestingly, these data reveal that while replacement of H<sub>c</sub> in **1b**[PF<sub>6</sub>] by a halogen atom in **2a,b**[PF<sub>6</sub>] has a sizable influence on the redox and ESR signatures of the Fe(III) radical (Table 2), this structural modification apparently does not modify significantly the spin distribution on the  $\pi$

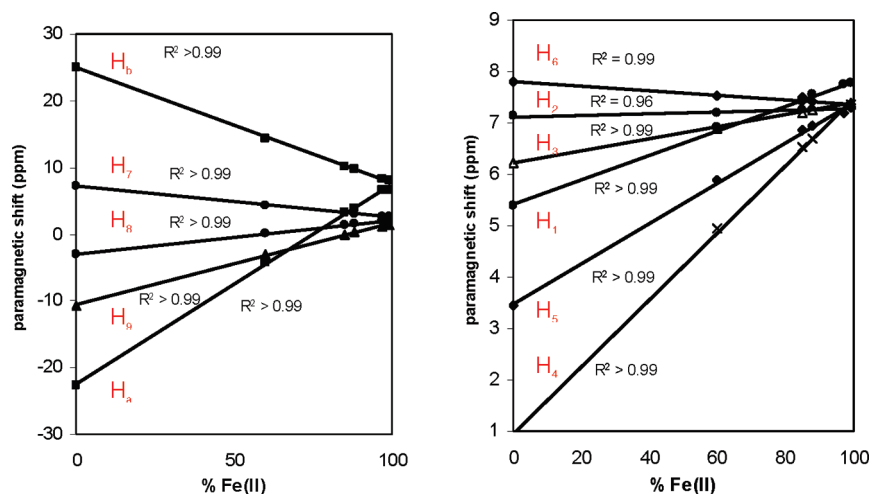
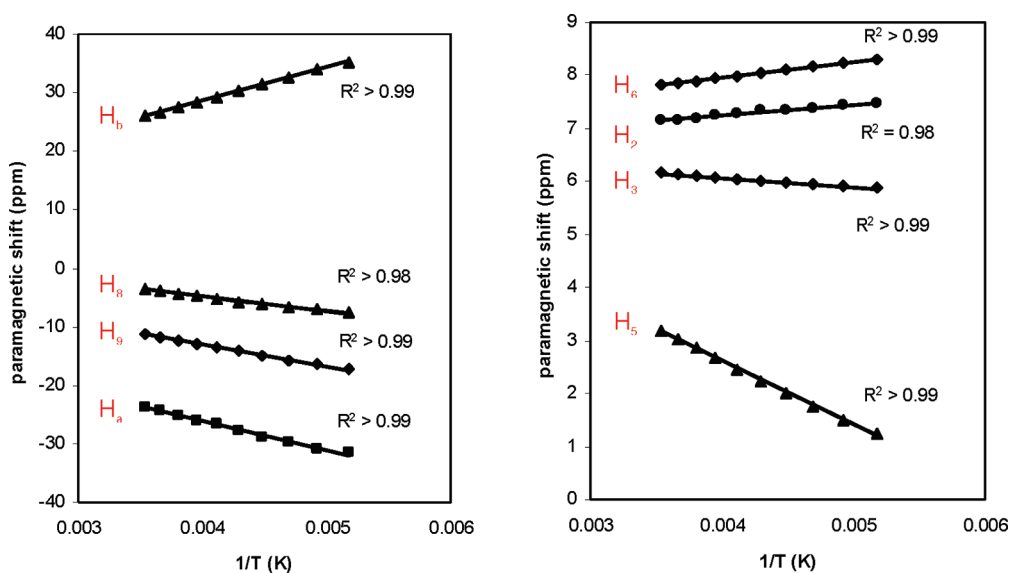
(21) Comparison between the bond distances between **2a,b** and **2a,b**[PF<sub>6</sub>] indicates only modest changes in geometry upon oxidation (Supporting Information).

(22)  $(Q_{\text{CH}})^{\text{H}}$  is a constant presently taken as -66 MHz.<sup>20</sup>

**Table 5.** Calculated Spin Densities ( $e$ ) on Selected Fragments or Atoms for  $[(\eta^2\text{-dpe})(\eta^5\text{-C}_5\text{H}_5)\text{FeC}\equiv\text{C}(x\text{-C}_5\text{H}_3\text{N})]^+$  Complexes (dpe = 1,2-Diphosphinoethane;  $x = 4, 3, 2$ ) in the Perpendicular and Parallel Conformations<sup>a</sup>

compd	Fe	C atom of C <sub>5</sub> H <sub>5</sub>	P atom of dpe	C≡C( <i>x</i> -C <sub>6</sub> H <sub>3</sub> N)								N	$\Delta E^b$ (kJ mol <sup>-1</sup> )	
				C <sub>a</sub>	C <sub>b</sub>	C <sub>c</sub>	C <sub>d</sub>	C <sub>e</sub>	C <sub>f</sub>	C <sub>g</sub>	C <sub>h</sub>			
<b>1a</b> -H <sup>+</sup>	$\parallel^c$	0.799	-0.003	-0.016	-0.054	0.299	-0.025	0.014	-0.001				0.002	9.1 <sup>e</sup>
( <i>n</i> = 4)	$\perp^d$	0.691	-0.002	-0.015	-0.026	0.246	-0.035	0.083	-0.032				0.075	0
<b>1b</b> -H <sup>+</sup>	$\parallel^c$	0.738	-0.003	-0.016	-0.041	0.271	-0.018	0.007	0.003	-0.003		0.010	0.067	14.4 <sup>e</sup>
( <i>n</i> = 3)	$\perp_1^d$	0.654	-0.002	-0.014	-0.009	0.233	-0.026	0.069	-0.032	0.109		0.094	-0.030	2.1
	$\perp_2^d$	0.648	-0.002	-0.014	-0.007	0.234	-0.026	0.070	-0.033	0.109		0.094	-0.030	0
<b>1c</b> -H <sup>+</sup>	$\parallel^c$	0.822	-0.003	-0.018	-0.067	0.303	-0.025	0.008	0.001	0.001	0.001		0.010	19.4 <sup>e</sup>
( <i>n</i> = 2)	$\perp_1^d$	0.673	-0.003	-0.014	-0.024	0.244	-0.036	0.097	-0.040	0.113	-0.016		0.045	8.9
	$\perp_2^d$	0.695	-0.002	-0.016	-0.033	0.240	-0.036	0.095	-0.038	0.108	-0.015		0.044	0

<sup>a</sup> See Chart 3 for atom numbering. <sup>b</sup> Relative energy between the conformations. <sup>c</sup> Parallel conformation. <sup>d</sup> Perpendicular conformation ( $\perp_1$ , nitrogen atom toward C<sub>5</sub>H<sub>5</sub> ligand;  $\perp_2$ , nitrogen atom away from C<sub>5</sub>H<sub>5</sub> ligand). <sup>e</sup> For this compound, see the computational details in the Experimental Section.

**Figure 4.** Observed <sup>1</sup>H NMR shifts for (a) **1a**/**1a**[PF<sub>6</sub>] mixtures in CD<sub>2</sub>Cl<sub>2</sub> at 25 °C (assignment according to Chart 2) and (b) aromatic protons of the dppe ligand.**Figure 5.** Temperature dependence of selected <sup>1</sup>H NMR shifts for **1a**[PF<sub>6</sub>] in CD<sub>2</sub>Cl<sub>2</sub> with proposed assignment according to Chart 2.

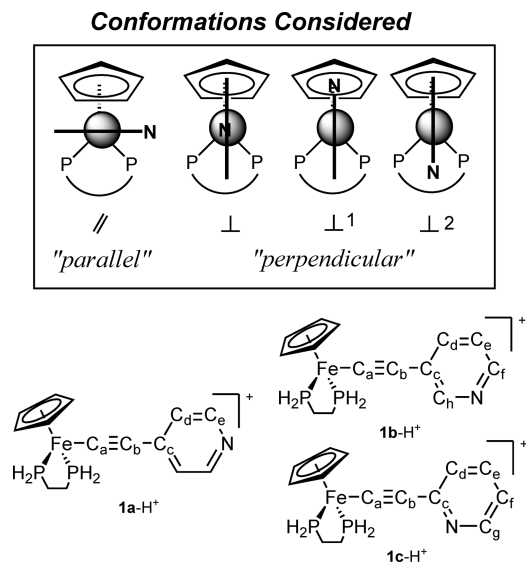
manifold of the pyridyl ring.

$$(A_{\text{H}})_{\text{con}} = \delta_c \hbar^3 \gamma_{\text{H}} k T / (g \mu_{\text{B}} S(S+1)) \quad (3)$$

$$(A_{\text{H}})_{\text{con}} / h = (Q_{\text{CH}})^{\text{H}} (\rho^{\pi})_{\text{C}} \quad (4)$$

**Theoretical Results.** DFT calculations were performed on the mononuclear Fe(II) and Fe(III) model complexes **1a**-H<sup>0/+</sup>, **1b**-H<sup>0/+</sup>, and **1c**-H<sup>0/+</sup>, in which the dppe and C<sub>5</sub>Me<sub>5</sub> ligands have been replaced by 1,2-diphosphinoethane (dpe) and C<sub>5</sub>H<sub>5</sub>, respectively. These complexes were optimized in

**Chart 3. Mononuclear Model Complexes Used in the DFT Calculations and Numbering Scheme Used**



several geometries corresponding to the various parallel and perpendicular conformations that the pyridyl group can adopt. Two conformations were considered for the  $1a-H^+$  complex: one where the aryl plane and the ethane bridge of the dpe ligand is roughly parallel,  $1a^{\parallel}-H^+$ , and one where the plane of the functional aryl ring roughly bisects the dpe and  $C_5H_5$  ligands,  $1a^{\perp}-H^+$  (Chart 3). Three conformations were considered for  $1b-H^+$  and  $1c-H^+$  (the nitrogen atom being out the aryl axis): a "parallel" conformation ( $1b^{\parallel}-H^+$  and  $1c^{\parallel}-H^+$ ) and two "perpendicular" conformations; one with the nitrogen atom pointing toward the cyclopentadienyl ligand ( $1b^{\perp 1}-H^+$  and  $1c^{\perp 1}-H^+$ ) and another one with the nitrogen atom pointing away from it ( $1b^{\perp 2}-H^+$  and  $1c^{\perp 2}-H^+$ ).

The "perpendicular" conformations of these model compounds were optimized without symmetry constraints, while the parallel conformation was imposed by constraining the involved dihedral angles, the geometry optimization process leading to one of the perpendicular structures. The parallel conformations are actually ca. 0.1–0.2 eV higher in energy than the most stable perpendicular one (Table 5). Surprisingly, a sizable difference in stability (ca. 0.1 eV) was found between  $1c^{\perp 1}-H^+$  and  $1c^{\perp 2}-H^+$ , revealing a non-negligible (electronic) influence of the nitrogen position in the ortho pyridyl complex. Notably, no such difference in stability was found in the meta isomer.

Energies of the frontier molecular spin-orbitals (SOs) for  $1a-H^+$ ,  $1b-H^+$ , and  $1c-H^+$  complexes in their most stable arrangement are shown in Figure 6. The presence of the nitrogen atom in the aromatic cycle modifies the usual energy scheme of the highest occupied spin-orbitals found in the series of  $3-X^+$  arylacetylide compounds previously studied. The lone pair of the nitrogen atom is energetically close to the "t<sub>2g</sub>" set of metallic orbitals (the discussion is based on a spin-restricted scheme for sake of clarity). Thus, depending on the pseudosymmetry of the nitrogen lone pair (position of the nitrogen atom in the conjugated ring), it can be found almost unchanged, as in  $1a-H^+$ , where it has a axial symmetry, or in an in-phase and out-of-phase combinations with the metallic "t<sub>2g</sub>" orbital of the same pseudosymmetry. This is illustrated in Table S5 of the Supporting Information by the plots of the frontiers SOs for each system.

The lowest unoccupied spin orbital or LUSO( $\beta$ ) has, in each case, a strong metallic d<sub>xz</sub> metallic character which also presents a non-negligible  $\pi$  pyridine character in the case of  $1b-H^+$  and  $1c-H^+$  (see Figure 6). The LUSO( $\alpha$ ) and LUSO+1( $\alpha$ ) and the corresponding LUSO+1( $\beta$ ) and LUSO+2( $\beta$ ) are strongly metallic in character and correspond to the well-known "e<sub>g</sub>" orbitals of a metallic system in a pseudo- $O_h$  symmetry. It has to be noted that this electronic structure is notably affected by a 90° rotation of the metallic fragment around the acetylide axis, in line with the rather large differences in energy found between both arrangements.

The ionization potentials have been derived for  $1a-c-H$  (Table 2) considering the most stable conformations for each redox state. The order for the ionization potentials computed for  $1a-c-H$  ( $1a-H \gg 1b-H > 1c-H$ ) does not follow the order of the redox potentials experimentally found for  $1a-c$  ( $1a \gg 1c > 1b$ ). While specific solvation or electrostatic interactions might explain this discrepancy for the last two isomers, these data nevertheless clearly confirm that oxidation of  $1a$  should be significantly more difficult than for the two other isomers, as experimentally observed.

The atomic spin densities are given in Table 5 for all studied conformations. Very close spin distributions are found for the two perpendicular conformations of  $1b-H^+$  and  $1c-H^+$ . In contrast, the spin distributions in the parallel conformations sensibly differ for all three Fe(III) model complexes. Nevertheless, this configuration is significantly higher in energy compared to the perpendicular arrangements ( $> 10 \text{ kJ mol}^{-1}$ ) and is thus less representative. The ESR  $g$  tensors were calculated for the cationic system in all arrangements (Supporting Information). They are given in Table 2 for the most stable structures (perpendicular). The  $g_{\text{iso}}$  value is in each case smaller than the experimental measurements ( $\sim 2.05\text{--}2.07$  compared to  $\sim 2.16$ ), and the anisotropy is less important ( $\sim 0.1\text{--}0.2$  compared to  $\sim 0.5$ ). These systematic deviations are mainly due to the simplification of the ligands in the coordination sphere of the metal,<sup>25b</sup> an effect also apparent in the lower atomic spin-density values found for  $1a-H^+$ ,  $1b-H^+$ , and  $1c-H^+$  (see later). The poor influence of the position of the nitrogen atom in the six-membered ring on the EPR  $g$  tensor experimentally stated (Table 2) is, however, well reproduced.

## Discussion

**Electronic Structures of  $1a-c[\text{PF}_6]$  and  $2a,b[\text{PF}_6]$ .** According to the present study,  $1a-c[\text{PF}_6]$  and  $2a,b[\text{PF}_6]$  constitute new examples of Fe(III) organometallic metal-centered radical cations.<sup>15</sup> Comparison of their ESR ( $g$ ,  $\Delta g$ ; Table 2), redox (Fe(III)/Fe(II) potentials; Table 2), and infrared ( $\nu_{\text{C}\equiv\text{C}}$ )<sup>5</sup> signatures with those previously determined for their  $3-X[\text{PF}_6]$  analogues reveals that the electronic effect of the pyridylalkynyl ligands is comparable to that exerted by 4-phenylalkynyl ligands functionalized by strongly electron-withdrawing groups, such as for instance  $3\text{-NO}_2[\text{PF}_6]$  or  $3\text{-CN}[\text{PF}_6]$ .<sup>8,11</sup> The metal-centered character of these radicals evidenced by Mössbauer and ESR spectroscopy is well rationalized by DFT computations on  $1a-H^+$ ,  $1b-H^+$ , and  $1c-H^+$ , which also indicate that sensibly similar spin densities are present on the metal center of the three model complexes, regardless of the appended pyridyl group (Table 4). Experimentally, the metallic character of the unpaired electron is also clearly indicated by

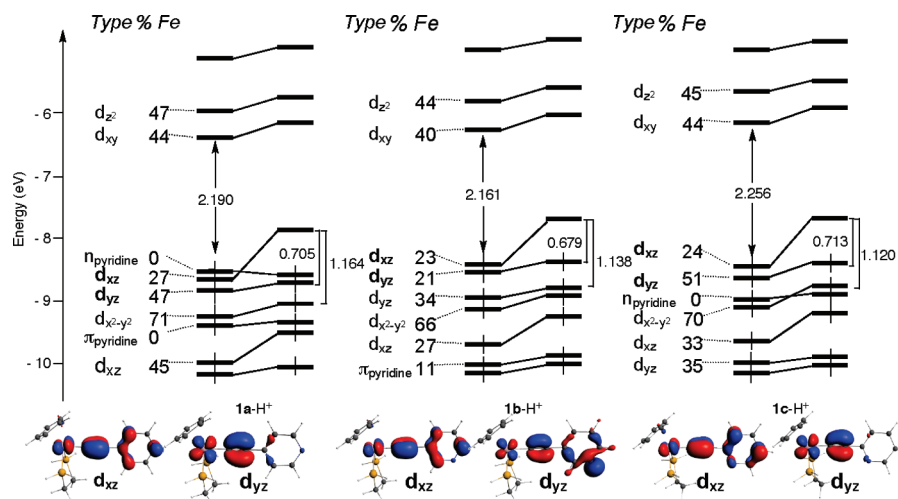
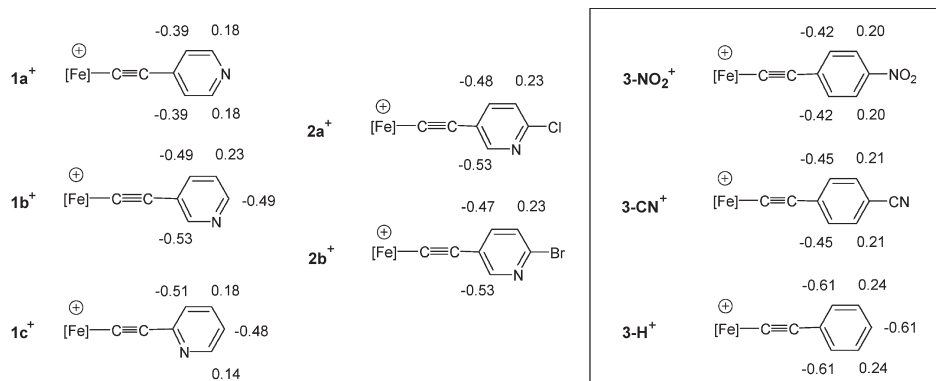


**Figure 6.** Energy diagram of the frontier spin-orbitals of the optimized systems **1a-H<sup>+</sup>**, **1b-H<sup>+</sup>**, and **1c-H<sup>+</sup>** in their most stable conformations. The percentage of metallic character is indicated for the  $\alpha$  SOs. The two highest occupied  $\alpha$  SOs are plotted (isocontour 0.05 [e/bohr<sup>3</sup>]<sup>1/2</sup>).

**Scheme 2. Comparison between the Contact Hyperfine Coupling Constants (in G) of Selected Hydrogen Atoms ( $A_{\text{H,con}}$ ) of **1a-c<sup>+</sup>** and **2a,b<sup>+</sup>** and of **3-NO<sub>2</sub><sup>+</sup>**, **3-CN<sup>+</sup>**, and **3-H<sup>+</sup>** (insert)**



the relatively large asymmetry of the rhombic ESR spectra observed for **1a-c[PF<sub>6</sub>]** ( $\Delta g \approx 0.53 \pm 0.01$ ).<sup>8</sup> Notably, this asymmetry is not very sensitive to the position of the nitrogen in the pyridyl heterocycle ( $\Delta g[\mathbf{1a}^+] \approx \Delta g[\mathbf{1b}^+] \leq \Delta g[\mathbf{1c}^+]$ ), in spite of the different nature/ordering of some of the frontier MOs presently evidenced for each isomer **1a<sup>+</sup>**, **1b<sup>+</sup>**, and **1c<sup>+</sup>**. A more apparent effect of the different electronic structures of these isomers is that the change in the ESR anisotropy along the **1a-c<sup>+</sup>** series is not related to the shifts between the Fe(III/II) potential redox potentials between the corresponding compounds ( $E^\circ[\mathbf{1a}^+] \geq E^\circ[\mathbf{1c}^+] \geq E^\circ[\mathbf{1b}^+]$ ), as previously observed across the **3-X<sup>+</sup>** series.<sup>8</sup> A similar statement can also be made when the ESR anisotropies and ionization potentials computed for the model complexes by DFT are considered (Table 2). However, between similar isomers such as the meta pyridyl complexes **1b[PF<sub>6</sub>]** and **2a,b[PF<sub>6</sub>]**, this proportionality is restored and the ESR anisotropy increases in the order of the oxidation potentials (Table 2). Actually, this electronic substituent effect is reminiscent of that previously observed among **3-H[PF<sub>6</sub>]**, **3-Cl[PF<sub>6</sub>]**, and **3-Br[PF<sub>6</sub>]**, albeit in a slightly less marked way.<sup>8</sup> Likewise, this effect can be related to an increase in the metallic character of the radical upon depressing the electron-releasing capabilities of the arylacetylide ligand by appending an electron-withdrawing substituent to the pyridyl ring of **1b[PF<sub>6</sub>]** in a para position. Finally, when closer atten-

tion is brought to **1a[PF<sub>6</sub>]**, possessing an axially symmetric pyridyl ligand, strong similarities between the UV-near-IR spectra of that compound and those of **3-NO<sub>2</sub>[PF<sub>6</sub>]** or **3-CN[PF<sub>6</sub>]** are found.<sup>8</sup> This further suggests that the low-lying excited states of all these Fe(III) complexes have rather similar energies and exhibit comparable transition moments, as expected for excited states involving (partly) forbidden LF transitions.

**Spin Distribution in **1a-c[PF<sub>6</sub>]** and **2a,b[PF<sub>6</sub>]**.** As revealed by the DFT calculations, most of the spin density resides on the metal center and a significant part also on the  $\beta$ -acetylide carbon atom (Table 5). However, a sizable positive spin density (up to ca. 10% of that present on the metallic center) is also present on the pyridyl rings. A precise account of the changes in spin distribution taking place on the pyridyl fragments between **1a-c[PF<sub>6</sub>]** and **2a,b[PF<sub>6</sub>]** can be gained from <sup>1</sup>H NMR studies (Table 4).<sup>23,24</sup> Indeed, according to McConnell (eq 4), the proton contact hyperfine coupling constants (Scheme 2) are proportional to the spin densities on the neighboring carbon atoms. From these experimental data, it appears more plainly than from ESR or Mössbauer data that

(23) Kaupp, M.; Köhler, F. H. *Coord. Chem. Rev.* **2009**, *253*, 2376–2386.

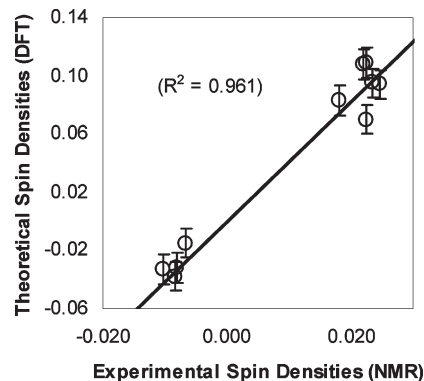
(24) Bertini, I.; Luchinat, C.; Parigi, G. *Solution NMR of Paramagnetic Molecules. Application to Metallobiomolecules and Models*; Elsevier: Amsterdam, 2001.

the positive spin density delocalized on the pyridylethynyl ligand of **1a-c**[PF<sub>6</sub>] depends primarily on the position of the nitrogen in the heterocycle. Unsurprisingly, the order found (meta > ortho > para) corresponds to the electron-releasing capability of the pyridyl ring previously evidenced by electrochemistry (Table 2). The positive spin densities found on the (hetero)aryl group for **1a-c**[PF<sub>6</sub>] are lower than those previously found for **3-H**[PF<sub>6</sub>], those for **1a**[PF<sub>6</sub>] closely resembling the densities previously found for **3-NO<sub>2</sub>**[PF<sub>6</sub>].<sup>7</sup> Interestingly, as mentioned above, the presence of a para halogen substituent on the pyridyl heterocycle does not seem to modify strongly the spin distribution on that fragment (Table 4). A marginal decrease of the positive spin density on C<sub>d</sub>, C<sub>e</sub>, and C<sub>f</sub> is indicated by the isotropic shifts of H<sub>a</sub>, H<sub>b</sub>, and H<sub>d</sub>, respectively, among the 3-pyridyl compounds (the order found is **2a**[PF<sub>6</sub>] ≈ **2b**[PF<sub>6</sub>] < **1b**[PF<sub>6</sub>]). This observation indicates that the mesomeric contribution due to the halogen substituent is not dominant over the inductive effect of the electropositive nitrogen atom within the pyridyl ring (Scheme 3). In line with related studies,<sup>8,25</sup> this indicates that the electronic influence of the nitrogen atom is in part inductively transmitted from the (functional) pyridyl rings to the metal center.

Regarding the experimental estimates of the spin densities found by NMR, a fair qualitative match is found with computed spin densities for **1a-H<sup>+</sup>**, **1b-H<sup>+</sup>**, and **1c-H<sup>+</sup>** in their most stable (perpendicular) conformation.<sup>23</sup> Indeed, considering a 0.01 e uncertainty on the DFT values, correct signs and relative magnitudes are retrieved by DFT for the atomic spin densities on the carbon atoms of the pyridyl ring (Figure 7). These spin densities are somewhat overestimated in the simplified model compounds used in the computations, but similar statements have been made before.<sup>7</sup> Considering the significant differences in spin density predicted by DFT between the parallel and perpendicular conformations, the experimental spin densities found for **1a-c**[PF<sub>6</sub>] suggest that essentially the perpendicular conformation of these Fe(III) radicals is present in solution at ambient temperature. This is indeed possible, since the latter corresponds to the most stable conformer for the model compounds (Supporting Information). Note that previous computations on **3-NO<sub>2</sub><sup>+</sup>** suggest that these energetic differences in stability might be less pronounced for the real compounds, due to the greater steric interactions taking place between the (hetero)aryl group and the C<sub>5</sub>Me<sub>5</sub> fragment in the perpendicular conformations.<sup>7</sup> However, the good Curie dependences stated for the various <sup>1</sup>H NMR isotropic shifts (Figure 5) further suggest that no conformational change takes place in the 100–300 K temperature range for **1a-c**[PF<sub>6</sub>]. Indeed, according to the DFT calculations, such a phenomenon should result in a marked change in the spin distribution on the pyridine fragments, which in turn would induce a departure from the good Curie behavior observed.<sup>26</sup>

(25) (a) Paul, F.; Ellis, B. J.; Bruce, M. I.; Toupet, L.; Roisnel, T.; Costuas, K.; Halet, J.-F.; Lapinte, C. *Organometallics* **2006**, *25*, 649–665. (b) Gauthier, N.; Tchouar, N.; Justaud, F.; Argouarch, G.; Cifuentes, M. P.; Toupet, L.; Touchard, D.; Halet, J.-F.; Rigaut, S.; Humphrey, M. G.; Costuas, K.; Paul, F. *Organometallics* **2009**, *28*, 2253–2266.

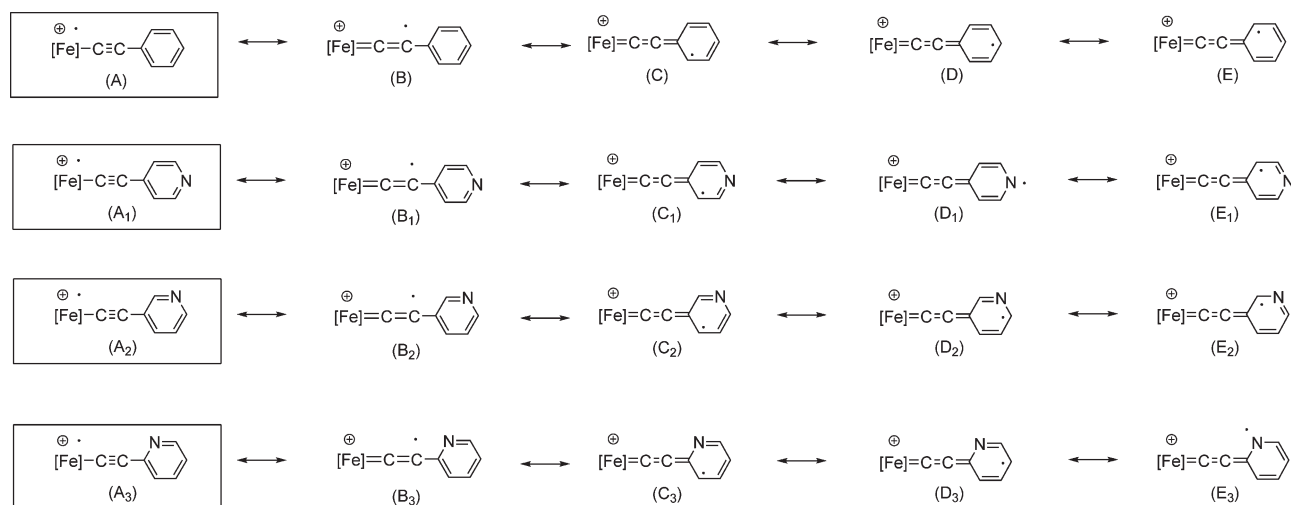
(26) See for instance: (a) Walter, M. D.; Berg, D. J.; Andersen, R. A. *Organometallics* **2007**, *26*, 2296–2307. (b) Walter, M. D.; Berg, D. J.; Andersen, R. A. *Organometallics* **2006**, *25*, 3228–3237. (c) Schultz, M.; Boncella, J. M.; Berg, D. J.; Tilley, T. D.; Andersen, R. A. *Organometallics* **2002**, *21*, 460–472.



**Figure 7.** Correlation of spin densities determined by <sup>1</sup>H NMR for selected carbon atoms of the pyridyl group for **1a**[PF<sub>6</sub>], **1b**[PF<sub>6</sub>]<sub>2</sub>, and **1c**[PF<sub>6</sub>] vs spin densities computed for the same atoms by DFT for **1a-H<sup>+</sup>**, **1b-H<sup>+</sup>**, and **1c-H<sup>+</sup>**. Vertical error bars represent the estimated uncertainty on the calculated spin densities (±0.01 e).

**Valence Bond (VB) Description of 1a-c[PF<sub>6</sub>].** When the experimental (Table 4) and theoretical (Table 5) spin distributions are analyzed in terms of valence bond (VB) structures (Scheme 3), it appears that the VB mesomers D<sub>1</sub> and E<sub>3</sub> have a negligible weight in the bonding description of **1a**[PF<sub>6</sub>] and **1c**[PF<sub>6</sub>]. This happens in **1a<sup>+</sup>** and **1c<sup>+</sup>** because the unpaired electron does not like to be strongly localized on the p<sub>z</sub> orbital of the nitrogen atom due to the stronger electronegativity of nitrogen relative to carbon. In contrast, for **1b<sup>+</sup>** and **2a,b<sup>+</sup>**, this radical cannot be located on nitrogen due to the symmetry of the SOMO. Accordingly, in these compounds, the spin densities found suggest that the VB structures C<sub>2</sub>–E<sub>2</sub> participate with quite comparable weights in the bonding description. The slightly greater spin density present on the pyridyl group could explain the greater kinetic instability found for **1b**[PF<sub>6</sub>] relative to **1a**[PF<sub>6</sub>] and **1c**[PF<sub>6</sub>]. Note that according to the available structural data for **2a**, **b**[PF<sub>6</sub>] the weight of VB mesomers B<sub>n</sub>–E<sub>n</sub> remains very small in the bonding description. The latter is obviously dominated by the VB A<sub>n</sub> mesomer (n = 1–3), in line with the strong localization of the electronic vacancy on the iron atom evidenced by DFT. The dominance of A<sub>1–3</sub> is also suggested by the infrared and the Mössbauer data. Indeed, while previous infrared measurements indicated only a modest shift of the triple-bond stretch to lower wavenumbers upon oxidation of **1a-c** in solution (Δν<sub>C≡C</sub> < 60 cm<sup>-1</sup>),<sup>5,11</sup> the present study reveals that these compounds exhibit a Mössbauer signature with a QS characteristic of Fe(III) alkynyl complexes without any indication of a marked cumulenic character.<sup>16</sup> This would not have been the case if the contribution of B<sub>n</sub>–D<sub>n</sub> (n = 1–3) was more pronounced.

**Conclusion.** This work reveals that the pyridylethynyl Fe(III) radicals **1a-c**[PF<sub>6</sub>] and **2a,b**[PF<sub>6</sub>] overall resemble their nonheterocyclic congeners **3-X<sup>+</sup>**, which bear a strongly electron-withdrawing substituent in a para position. In **1a-c**[PF<sub>6</sub>], it is the nitrogen atom present in the pyridyl rings which qualitatively replaces this substituent, by virtue of its large electronegativity. However, a closer inspection of the various spectroscopic and redox signatures of these organometallic radicals reveals that the electronic substituent effect of the heterocycle cannot be reduced to a single parameter across the **1a-c**[PF<sub>6</sub>] series. Indeed, the heteroaryl rings appear to influence in different ways the characteristic

**Scheme 3.** VB Representation of the Substituent-Dependent Delocalization of the Unpaired Electron in  $1a-c^+$  Complexes vs That in  $3-H^+$  ( $[Fe] = (\eta^2\text{-dppc})(\eta^5\text{-C}_5\text{Me}_5)\text{Fe}$ )

electronic/bonding parameters probed by these experimental techniques for each isomer.

Importantly, the present study reveals that beside the many spectroscopic techniques traditionally used to characterize radical cations,  $^1\text{H}$  NMR constitutes an interesting complementary method. Indeed, Mössbauer, ESR, and UV–vis–near-IR are poorly suited to experimentally investigate small electronic differences in spin distribution on the ligand for these metal-centered organometallic radicals. In contrast,  $^1\text{H}$  NMR proves much more sensitive to the electronic perturbations localized on the pyridyl group and allows unambiguous distinction between these paramagnetic isomers. Furthermore, this technique provides an accurate picture of the spin distribution on the heterocyclic ring, which is qualitatively reproduced by DFT calculations performed on simpler models. On the basis of these results, NMR spectroscopy appears perfectly suited to empirically address slight electronic changes such as those brought by coordination of the nitrogen lone pair to a Lewis-acidic site and will be used accordingly in future investigations aimed at examining complexation reactions of these Fe(III) metallo-ligands.

### Experimental Section

**General Data.** All manipulations were carried out under an inert atmosphere. Solvents or reagents were used as follows:  $\text{Et}_2\text{O}$  and  $n$ -pentane, distilled from Na/benzophenone;  $\text{CH}_2\text{Cl}_2$ , distilled from  $\text{CaH}_2$  and purged with argon, opened/stored under Ar. The  $[(\eta^5\text{-C}_5\text{H}_5)_2\text{Fe}][\text{PF}_6]$  ferrocenium salt was prepared by previously published procedures.<sup>27</sup> Transmittance-FTIR spectra were recorded using a Bruker IFS28 spectrometer ( $400\text{--}4000\text{ cm}^{-1}$ ). UV–visible and near-infrared (near-IR) spectra were recorded using a Cary 5000 spectrometer. All NMR experiments were performed on a Bruker AVANCE 500 instrument operating at 500.15 MHz for  $^1\text{H}$  and 125.769 MHz for  $^{13}\text{C}$ , with a 5 mm broad-band observe probe equipped with a z-gradient coil (Supporting Information). ESR spectra were recorded on a Bruker EMX-8/2.7 (X-band) spectrometer. Cyclic voltammograms were recorded using a EG&G potentiostat (M.263) on platinum electrodes referenced to an SCE electrode and were calibrated with the  $[\text{FcH}]/[\text{FcH}]^+$  couple taken at 0.46 V in  $\text{CH}_2\text{Cl}_2$ .<sup>27</sup> The  $^{57}\text{Fe}$  Mössbauer spectra were recorded

at the LCC (Toulouse, France). They were obtained by using a constant acceleration spectrometer previously described with a 50 mCi  $^{57}\text{Co}$  source in a Rh matrix.<sup>28</sup> The sample temperature was controlled by an Oxford MD306 cryostat and an Oxford ITC4 temperature controller. Computer fitting of the Mössbauer data to Lorentzian line shapes was carried out with a previously reported computer program.<sup>29</sup> The isomer shift values are reported relative to iron foil at 298 K and are not corrected for the temperature-dependent second-order Doppler shift. The Mössbauer sample cell consists of a 2 cm diameter cylindrical Plexiglas holder. The complexes  $1a-c[\text{PF}_6]_2^5$  and  $2a,b^3$  were obtained as previously reported.

**General Procedure for the Synthesis of the Mononuclear Fe(III) Alkynyl Complexes  $2a[\text{PF}_6]$  and  $2b[\text{PF}_6]$ .** A 0.95 equiv amount of  $[\text{Fe}(\eta^5\text{-C}_5\text{H}_5)_2][\text{PF}_6]$  (0.040 g; 0.120 mmol) was added to a solution of the corresponding Fe(II) precursor (0.125 mmol) in 10 mL of dichloromethane. An instantaneous darkening of the solution was observed. Stirring was maintained for 1 h at room temperature, and the solution was concentrated in vacuo to approximately 2 mL. Addition of 25 mL of  $n$ -pentane allowed precipitation of a dark solid. Decantation and subsequent washing with  $3 \times 3\text{ mL}$  portions of toluene followed by  $3 \times 3\text{ mL}$  diethyl ether and drying under vacuum yielded the desired complex. Both compounds were crystallized as dark rhombic cubes by slow diffusion of  $n$ -pentane into a dichloromethane solution of the compound.

$[(\eta^2\text{-dppc})(\eta^5\text{-C}_5\text{Me}_5)\text{FeC}\equiv\text{C}\{5\text{-}(2\text{-C}_6\text{H}_3\text{N}_1\text{Cl}_1)\}][\text{PF}_6]$  ( $2a[\text{PF}_6]$ ). Yield: 83%. Color: dark gray. IR ( $\nu$ , KBr,  $\text{cm}^{-1}$ ): 2009 (vw), 1945 (m,  $\text{C}\equiv\text{C}$ ). UV–Vis–near-IR ( $\text{CH}_2\text{Cl}_2$ ;  $\lambda_{\text{max}}$  ( $\epsilon/10^3\text{ dm}^3\text{ M}^{-1}\text{ cm}^{-1}$ )): 312 (sh, 13.45); 380 (sh, 2.81); 560 (1.52); 635 (1.46); 1900 (0.08).

$[(\eta^2\text{-dppc})(\eta^5\text{-C}_5\text{Me}_5)\text{FeC}\equiv\text{C}\{5\text{-}(2\text{-C}_6\text{H}_3\text{N}_1\text{Br}_1)\}][\text{PF}_6]$  ( $2b[\text{PF}_6]$ ). Yield: 84%. Color: dark gray. IR ( $\nu$ , KBr,  $\text{cm}^{-1}$ ): 2004 (vw), 1946 (w,  $\text{C}\equiv\text{C}$ ). UV–Vis–near-IR ( $\text{CH}_2\text{Cl}_2$ ;  $\lambda_{\text{max}}$  ( $\epsilon/10^3\text{ dm}^3\text{ M}^{-1}\text{ cm}^{-1}$ )): 314 (sh, 14.32); 380 (sh, 3.39); 562 (1.77); 636 (1.66); 1900 (0.08).

**Crystallography.** Crystals of  $2a,b[\text{PF}_6]$  were obtained as described above. The samples were studied on a Sapphire 3 Xcalibur CCD instrument with graphite-monochromated Mo  $\text{K}\alpha$  radiation. The cell parameters were obtained with Denzo and Scalepack with 10 frames ( $\psi$  rotation:  $1^\circ$  per frame).<sup>30</sup> The

(28) Boinnard, D.; Bousseksou, A.; Dworkin, A.; Savariault, J.-M.; Varret, F.; Tuchagues, J.-P. *Inorg. Chem.* **1994**, *33*, 271.

(29) Varret, F.; Mariot, J.-P.; Hamon, J.-R.; Astruc, D. *Hyperfine Interact.* **1988**, *39*, 67.

(30) Otwinowski, Z.; Minor, W. In *Methods in Enzymology*; Carter, C. W., Sweet, R. M., Eds.; Academic Press: London, 1997; Vol. 276, pp 307–326.

**Table 6. Crystal Data and Data Collection and Refinement Parameters for 2a[PF<sub>6</sub>] and 2b[PF<sub>6</sub>]**

	2a[PF <sub>6</sub> ]	2b[PF <sub>6</sub> ]
formula	C <sub>43</sub> H <sub>43</sub> Cl <sub>1</sub> N <sub>1</sub> - P <sub>2</sub> Fe <sub>1</sub> ,PF <sub>6</sub>	C <sub>43</sub> H <sub>43</sub> Br <sub>1</sub> N <sub>1</sub> - P <sub>2</sub> Fe <sub>1</sub> ,PF <sub>6</sub>
fw	870.99	915.45
temp (K)	120(2)	150(2)
cryst syst	monoclinic	monoclinic
space group	<i>P</i> 2 <sub>1</sub> / <i>c</i>	<i>P</i> 2 <sub>1</sub> / <i>c</i>
<i>a</i> (Å)	17.3677(5)	17.5014(5)
<i>b</i> (Å)	12.6604(4)	12.8073(4)
<i>c</i> (Å)	18.3312(4)	18.3184(4)
α (deg)	90.0	90.0
β (deg)	93.827(2)	94.169(2)
γ (deg)	90.0	90.0
V(Å <sup>3</sup> )	4021.71(19)	4095.1(2)
Z	4	4
<i>D</i> <sub>calcd</sub> (g cm <sup>-3</sup> )	1.438	1.485
cryst size (mm)	0.30 × 0.25 × 0.12	0.24 × 0.20 × 0.14
<i>F</i> (000)	1796	1868
diffractometer	CCD Sapphire 3 Xcalibur	CCD Sapphire 3 Xcalibur
radiation	Mo Kα	Mo Kα
abs coeff (mm <sup>-1</sup> )	0.621	0.711
θ range (deg)	2.75–27.00	2.59–27.00
<i>hkl</i> range	–22 to +22 –15 to +14 –23 to +23	–21 to +21 –16 to +16 –23 to +23
total no. of rflns	51 394	54 715
no. of obsd rflns ( <i>I</i> > 2σ( <i>I</i> ))	6852	8474
no. of restraints/params	0/496	0/496
final <i>R</i>	0.035	0.039
<i>R</i> <sub>w</sub>	0.098	0.066
<i>R</i> indices (all data)	0.046	0.101
<i>R</i> <sub>w</sub> (all data)	0.101	0.072
goodness of fit/ <i>F</i> <sup>2</sup> ( <i>S</i> <sub>w</sub> )	0.988	0.693

data collection<sup>31</sup> (Table 6) provided reflections for **2a,b**[PF<sub>6</sub>]. Subsequent data reduction with Denzo and Scalepack<sup>30</sup> gave the independent reflections (Table 6). The structures were solved with SIR-97, which revealed the non-hydrogen atoms.<sup>32</sup> After anisotropic refinement, the remaining atoms were found in Fourier difference maps. The complete structures were then refined with SHELXL97<sup>33</sup> by the full-matrix least-squares technique (use of *F*<sup>2</sup> magnitude; *x*, *y*, *z*, β<sub>ij</sub> for Fe, P, C, N, and/or O atoms, *x*, *y*, *z* in riding mode for H atoms with variables *N*(var), observations and *w* used as defined in Table 6). Atomic scattering factors were taken from the literature.<sup>34</sup> ORTEP views of **2a,b**[PF<sub>6</sub>] were obtained with PLATON98.<sup>35</sup>

**DFT Calculations.** DFT calculations were carried out using the Amsterdam Density Functional (ADF) program.<sup>36</sup> The model compounds [(η<sup>2</sup>-dpe)(η<sup>5</sup>-C<sub>5</sub>H<sub>5</sub>)FeC≡C(*x*-C<sub>6</sub>H<sub>3</sub>N)]<sup>*n*+</sup> (dpe = 1,2-diphosphinoethane; *x* = 4, 3, 2) labeled **1a-H<sup>*n*+</sup>**,

and **1a-H<sup>*n*+</sup>** (*n* = 0, 1), respectively, were used in order to reduce computational effort. Electron correlation was treated within the local density approximation (LDA) in the Vosko–Wilk–Nusair parametrization.<sup>37</sup> The nonlocal corrections of Becke<sup>38</sup> and of Perdew<sup>39</sup> were added to the exchange and correlation energies, respectively. The numerical integration procedure applied for the calculations was developed by te Velde et al.<sup>40</sup> The standard ADF TZP basis set was used: i.e., a triple-ζ Slater-type orbital (STO) basis for Fe 3d and 4s and a single-ζ function for 4p of Fe. A triple-ζ STO basis set was employed for H 1s, for 2s and 2p of C and N, and for 3s and 3p of P extended with a single-ζ polarization function (2p for H; 3d for C, N, and P). Orbitals up to 1s, 2p, and 4p were kept frozen for C and N, for P, and for Fe, respectively. Full geometry optimizations (assuming *C*<sub>1</sub> symmetry) were carried out on each complex, using the analytical gradient method implemented by Versluis and Ziegler.<sup>41</sup> Geometry optimization convergence criteria were more drastic than default criteria (energy change < 0.0005 hartree, atomic position displacement < 0.005 Å). For the cationic systems, the parallel configuration was obtained by restraining the torsion angle between the plane of the pyridyl group and the P–Fe–P plane. Spin-unrestricted calculations were performed for all the open-shell systems considered. The Cartesian coordinates of the optimized geometries are given as Supporting Information. The EPR *g* tensor calculations were calculated as implemented in ADF.<sup>42</sup> In this case, the functional PBE was used,<sup>43</sup> and relativistic corrections were taken into account using the ZORA (zeroth order regular approximation) spin–orbit Hamiltonian with the appropriate basis set.<sup>44</sup> Representations of the molecular structures, orbitals, and spin densities were done using MOLEKEL4.3<sup>45</sup> and ADF-GUI.<sup>46</sup>

**Acknowledgment.** A. Mari (LCC, Toulouse, France) is acknowledged for Mössbauer measurements. The MNERT (Ph.D. grant to F.M.), Region Bretagne (Ph. D. grant to G.d.C.), CNRS and ATCO (Ph.D. grant to S.L.S.) are acknowledged for financial support. The theoretical calculations were performed using HPC resources from GENCI CINES and GENCI IDRIS (Grant 2009-[x2010080649]). Dr. Katy Green is acknowledged for editorial help.

**Supporting Information Available:** Text, figures, and tables giving additional NMR data for **1a–c**[PF<sub>6</sub>], derivation of spin densities for selected aromatic protons based on isotropic shifts, changes for selected bond lengths and angles between **2a,b** and **2a,b**[PF<sub>6</sub>], Cartesian coordinates and total bonding energies of

- (31) *Kappa CCD Software*; Nonius BV, Delft, The Netherlands, 1999.  
 (32) Altomare, A.; Burla, M. C.; Camalli, M.; Cascarano, G.; Giacovazzo, C.; Guagliardi, A.; Moliterni, A. G. G.; Polidori, G.; Spagna, R. *J. Appl. Chem.* **1998**, *31*, 74–77.  
 (33) Sheldrick, G. M. *SHELXL97-2: Program for the Refinement of Crystal Structures*; University of Göttingen, Göttingen, Germany, 1997.  
 (34) *International Tables for X-ray Crystallography*; Kynoch Press (present distributor D. Reidel, Dordrecht, The Netherlands): Birmingham, U.K., 1974; Vol. IV.  
 (35) Spek, A. L. *PLATON: A Multipurpose Crystallographic Tool*; Utrecht University, Utrecht, The Netherlands, 1998.  
 (36) (a) *SCM, ADF 2007.01 ed.*; Theoretical Chemistry, Vrije Universiteit, Amsterdam, The Netherlands, 2007. *SCF, ADF 2008.01*; Theoretical Chemistry, Vrije Universiteit, Amsterdam, The Netherlands, 2008. (b) te Velde, G.; Bickelhaupt, F. M.; Fonseca Guerra, C.; van Gisbergen, S. J. A.; Baerends, E. J.; Snijders, J.; Ziegler, T. *Theor. Chem. Acc.* **2001**, *22*, 931–967.

- (37) Vosko, S. D.; Wilk, L.; Nusair, M. *Can. J. Chem.* **1990**, *58*, 1200–1211.  
 (38) (a) Becke, A. D. *J. Chem. Phys.* **1986**, *84*, 4524–4529. (b) Becke, A. D. *Phys. Rev. A* **1988**, *38*, 3098–3100.  
 (39) Perdew, J. P. *Phys. Rev. B* **1986**, *33*, 8822–24.  
 (40) te Velde, G.; Baerends, E. J. *J. Comput. Phys.* **1992**, *99*, 84–98.  
 (41) Versluis, L.; Ziegler, T. *J. Chem. Phys.* **1988**, *88*, 322–328.  
 (42) (a) Schreckenbach, G.; Ziegler, T. *J. Phys. Chem. A* **1997**, *101*, 3388–3399. (b) van Lenthe, E.; van der Avoird, A.; Wormer, P. E. S. *J. Chem. Phys.* **1997**, *107*, 2488–2498.  
 (43) (a) Hammer, B.; Hansen, L. B.; Norskov, J. K. *Phys. Rev. B* **1999**, *59*, 7413–7421. (b) Perdew, J. P.; Burke, K.; Ernzerhof, M. *Phys. Rev. Lett.* **1996**, *77*, 3865–3868.  
 (44) (a) van Lenthe, E.; Baerends, E. J.; Snijders, J. G. *J. Chem. Phys.* **1993**, *99*, 4597–4610. (b) van Lenthe, E.; Baerends, E. J.; Snijders, J. G. *J. Chem. Phys.* **1994**, *101*, 9783–9792. (c) van Lenthe, E.; Ehlers, A. E.; Baerends, E. J. *J. Chem. Phys.* **1999**, *110*, 8943–8953.  
 (45) Flükiger, P.; Lüthi, H. P.; Portmann, S.; Weber, J. *MOLEKEL4.3*; Swiss Center for Scientific Computing (CSCS), 2001.  
 (46) *ADF-GUI*; SCM, Amsterdam, The Netherlands, 2008; www.scm.com.

all DFT optimized geometries for **1a**-H<sup>0/+</sup>, **1b**-H<sup>0/+</sup>, and **1c**-H<sup>0/+</sup>, contour plots of the frontier spin-orbitals of **1a-c**-H<sup>+</sup>, and calculated **g** tensors of **1a-c**-H<sup>+</sup> in different conformations and CIF files giving crystallographic data for **2a,b**[PF<sub>6</sub>]. This material is available free of charge via the Internet at <http://pubs.acs.org>. Final atomic positional coordinates, with

estimated standard deviations, bond lengths and angles, and anisotropic thermal parameters, have also been deposited at the Cambridge Crystallographic Data Centre and were allocated the deposition numbers CCDC 730944 and CCDC 745013, respectively. Ordering information is given on any current masthead page.